Efficient modeling of plasmonic organic hybrid electro/optic modulators

PROCEEDINGS OF SPIE

SPIEDigitalLibrary.org/conference-proceedings-of-spie

Efficient modeling of plasmonic organic hybrid electro/optic modulators

Tibaldi, Alberto, Ghomashi, Mohammadamin, Bertazzi, Francesco, Vallone, Marco, Goano, Michele, et al.

Alberto Tibaldi, Mohammadamin Ghomashi, Francesco Bertazzi, Marco Vallone, Michele Goano, Giovanni Ghione, "Efficient modeling of plasmonic organic hybrid electro/optic modulators," Proc. SPIE 11680, Physics and Simulation of Optoelectronic Devices XXIX, 1168003 (30 April 2021); doi: 10.1117/12.2581278

SPIE.

Event: SPIE OPTO, 2021, Online Only

Efficient Modeling of Plasmonic Organic Hybrid Electro/Optic Modulators

Alberto Tibaldi[a,b], Mohammadamin Ghomashi[b], Francesco Bertazzi[a,b], Marco Vallone[a], Michele Goano[a,b], and Giovanni Ghione[a]

[a]Dipartimento di Elettronica e Telecomunicazioni, Politecnico di Torino, Corso Duca degli Abruzzi 24, 10129 Torino (TO), Italia
[b]Istituto di Elettronica e di Ingegneria dell'Informazione e delle Telecomunicazioni, Consiglio Nazionale delle Ricerche c/o Politecnico di Torino

ABSTRACT

The work focuses on the modeling and simulation of plasmonic organic hybrid electro/optic modulators. Preliminary multiphysics-augmented simulations of the slot plasmonic waveguide phase modulator are presented. Instead of applying them to system-level models, they are combined with the results of 3D finite-difference time-domain (FDTD) simulations to achieve realistic physics-based simulations at moderate computational costs. The model is demonstrated on a Mach-Zehnder plasmonic modulator inspired to literature results and validated through a comparison with 3D-FDTD simulations of the entire device.

Keywords: Plasmonics, Optical polymers, Electrooptic effects, Electrooptic modulation, Mode matching methods, Finite difference methods

1. INTRODUCTION

Plasmonic organic hybrid (POH) electro-optic (E/O) modulators for 1.3 μm and 1.55 μm communication systems have been extensively studied during the last few years as an advanced solution for optical modulation within the silicon photonics framework.[1–3] Indeed, they exhibit outstanding modulator performances (albeit with quite large optical insertion losses) thanks to their non-diffraction limited characteristics, nanometer scale cross-sections,[4] micron scale total lengths and exceptional E/O material characteristics.[5] POH modulators exploit polymer-based E/O materials consisting of chromophore molecules dispersed in a host medium, which are previously oriented according to a static poling electric field.[6,7] Modulation of the material refractive index is performed by imposing an RF electric field to the poled material. The E/O material fills the phase shifter slots, which are designed to support plasmonic modes.[8] Thanks to the nanometer slot widths, very large RF electric fields can be obtained with low applied voltages, thus enhancing the E/O effect.

¿From the modeling standpoint, these devices are characterized by two fundamental challenges. The first one is describing the E/O effect on the basis of a multiphysics treatment, where the electro-optic modulation is evaluated from RF electrical simulations and is later used to obtain a complex, position-dependent and anisotropic refractive index profile adopted as input of the optical model. The second is achieving an accurate and efficient optical simulation framework. In this view, simplified optical models could exploit 2D modal simulations to obtain the modulator static response. Yet, such an approach cannot be used to simulate some of the device figures of merit, such as the extinction ratio or the insertion loss. Predicting these quantities would require a 3D full-wave model of the entire geometry, which is very challenging because of the extremely severe memory and computational requirements. In this work we present an intermediate approach between full 3D simulations and 2D modal simulations, applied to a POH E/O Mach-Zehnder modulator (MZM) design from the literature. Having identified the MZM response with that of a bimodal Fabry-Pérot interferometer, it is possible to accurately reconstruct the device static response by combining a single (without RF field) 3D finite difference time domain (FDTD) simulation and some (computationally inexpensive) mode simulations of 2D cross sections.

Further author information: (Send correspondence to Alberto Tibaldi)
Alberto Tibaldi: E-mail: alberto.tibaldi@polito.it, Telephone: +39 011 090 4082

Physics and Simulation of Optoelectronic Devices XXIX, edited by Bernd Witzigmann, Marek Osiński, Yasuhiko Arakawa, Proc. of SPIE Vol. 11680, 1168003 · © 2021 SPIE
CCC code: 0277-786X/21/$21 · doi: 10.1117/12.2581278

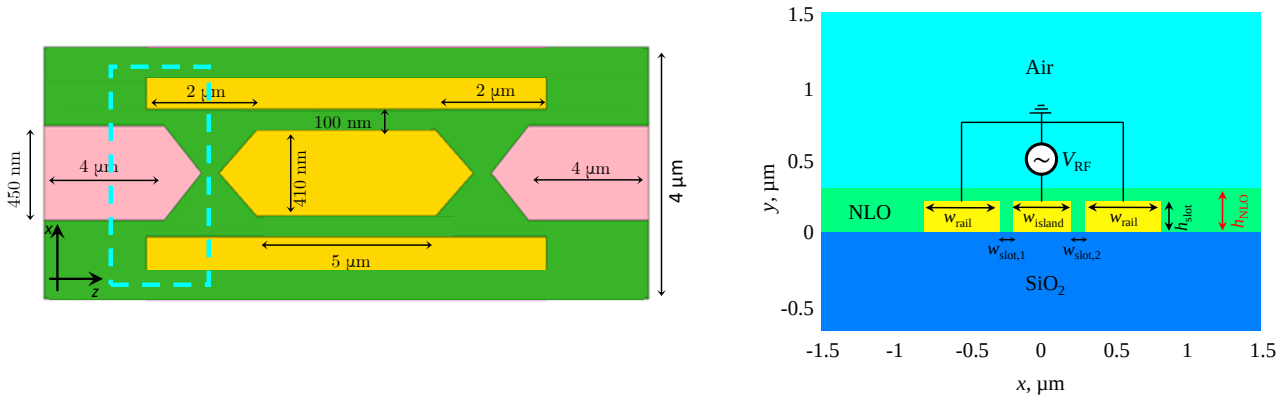

Figure 1. Sketch of the device under study, including the most relevant details. Left: top view. Right: cross-section in the phase modulator, including a schematic of the RF circuit enforcing the electro/optic effect.

The methodologies presented in this work are applied to a POH E/O MZ modulator similar to that presented in.[9] Figure 1 shows a top view (left) and a cross-section (right) of the device under study. The device is symmetric with respect to its central xy cut, so that the input and output sections have the same extent. The input signal is assumed to be the fundamental mode of the input (left) Si waveguide, represented in pink; in a dual fashion, the output signal is extracted from the right waveguide. In the splitter (and recombiner), the dielectric waveguide mode is converted into the plasmonic modes supported by the phase modulators (and viceversa), which are realized as slot waveguides embedded within the central gold island and the lateral gold rails. The slot height h_{slot} is 220 nm, while the width w_{slot} is designed to be 100 nm, which, being quite small allows to maximize the slot electric field and emphasize the E/O effect. From the cross-section in the right panel it is shown that the structure is fabricated on a SiO_2 layer, 3 μm thick; this is grown on a Si substrate, which is not shown in the figure but included in the RF simulations. Then, the device is filled with DLD-164, a non-linear optic (NLO) polymer ($n_{\text{NLO}} = 1.83$ at $\lambda = 1.55\mu$m,[10] total height, with total thickness $h_{\text{NLO}} = 300$ nm.

2. WAVEGUIDE SIMULATIONS

A simple though widely adopted simulation framework for POH E/O MZ modulators consists in limiting the analysis domain to the device cross-section, thus leading to modal waveguide simulations. The RF voltage, applied on the central island as in Fig. 1(right), induces an electric field that modulates the refractive index of the NLO polymer due to the Pockels effect. Therefore, the electro-optic effect can be described as

$$\Delta n_{\text{NLO}} = \frac{1}{2} r_{33} n_{\text{NLO}}^3 \,\text{sign}\,(x) \sqrt{|E_{x,\text{RF}}|^2 + |E_{y,\text{RF}}|^2}, \tag{1}$$

where r_{33} is the component of the E/O tensor (in contracted index notation) that perturbs n_{NLO} due to an RF electric field applied along the poling direction (consider that in a quasi-TEM approximation the RF and DC field patterns coincide), and $\text{sign}\,(x)$ takes into account that it has opposite signs in the two slots (refer to the RF circuit sketched in Fig. 1(right)). It is understood how (1) entails a multiphysics treatment, since the position-dependent $E_{x,\text{RF}}$, $E_{y,\text{RF}}$ field components should be derived through electrical simulations. Then, they should be interpolated on the optical problem mesh to evaluate Δn_{NLO} in its cross-section (the one simulated to produce Fig. 1(right)), thus requiring a coupled, multiphysics approach. To simplify the model, recalling that in MIM waveguides plasmonic modes are TM, with a dominant transverse component of the optical field, and that the RF field in the slots is mainly orthogonal to the slot walls, *i.e.,* only the perpendicular (x) component survives, the following approximation is sometimes adopted (see, *e.g.,*[5]):

$$\begin{aligned} \Delta n_{\text{NLO}} &\simeq \frac{1}{2} r_{33} n_{\text{NLO}}^3 \,\text{sign}\,(x)\, |E_{x,\text{RF}}|^2 \\ &\simeq \frac{1}{2} r_{33} n_{\text{NLO}}^3 \,\text{sign}\,(x)\, \frac{V_{\text{RF}}}{w_{\text{slot}}}, \end{aligned} \tag{2}$$

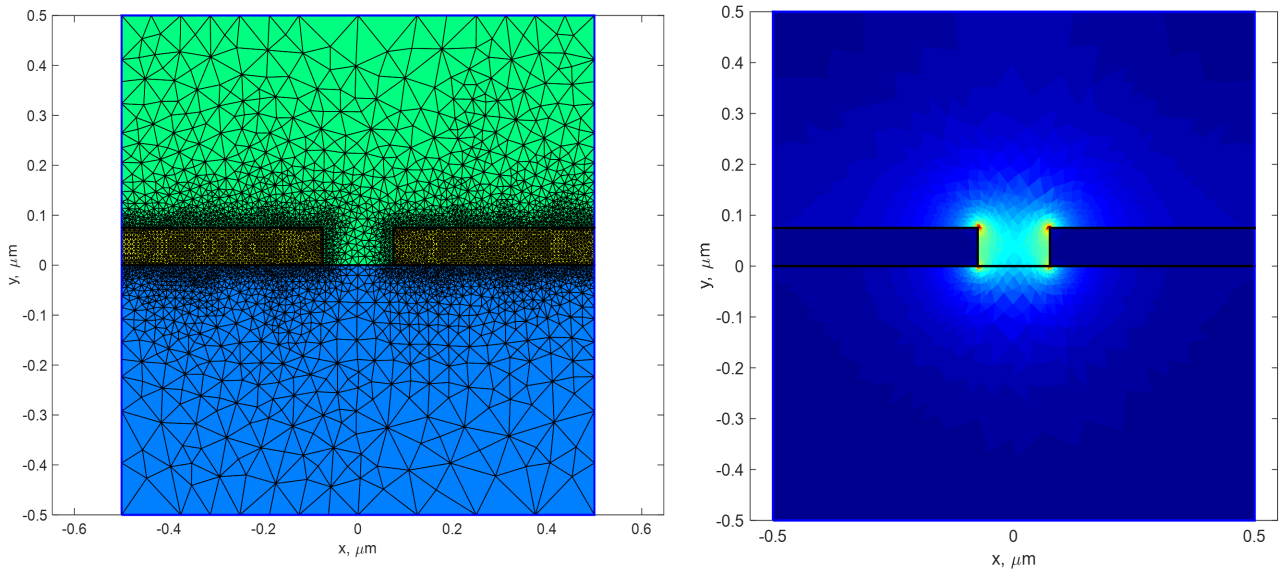

Figure 2. Left: example of finite element mesh for the optical simulation. Right: example of electric field magnitude of the optical mode of a slot waveguide.

yielding a constant, non-zero Δn_{NLO} only in the slot.

In this work the optical waveguide simulations have been performed by means of an in-house electromagnetic mode solver based on the finite element method (FEM).[11] Figure 2 shows examples of outputs of this software. On the left a typical mesh profile is reported. It can be noticed how the mesh is strongly refined at the metal-dielectric interfaces, in order to capture the characteristic steep variations of the optical field appreciable from the right panel, which reports an example of optical field magnitude. The other output of the solver is the modal complex refractive index. This is reported in Fig. 3 as a function of the RF voltage. The characteristics exhibit an anticrossing-like behaviour, which is peculiar of coupling between the slot modes.[12,13] The quasi-ON state is at $V_{\mathrm{RF}} = 0\,\mathrm{V}$, as it could be expected from symmetric modulators (equal slots). Each point of the characteristics has been obtained by simulating the waveguide with a different Δn_{NLO}. The figure shows two groups of curves, indicated in blue and red, which have been computed for two approximations of (1): for the blue curve, the electro-optic effect has been evaluated from electrical quasi-static simulations,[14] while the red curves are based on (2), which underestimates the electro-optic effect, thus affecting the prediction of V_π.

3. COMBINING FDTD AND WAVEGUIDE SIMULATIONS

Waveguide simulations allow to assess some of the figures of merit of a modulator, such as the V_π voltage. Still, they provide no estimate of the other relevant device figures of merit, *i.e.,* the insertion loss (IL) and the extinction ratio (ER). These could be in principle obtained by simple system-level models.[15] However, the realism of such an approach - basically, a trade-off between model simplicity and number of effects accounted for[13] - is somewhat questionable. In particular, so far no information about the slot mode topographies have been considered, as well as their interaction with the splitter and recombiner sections, which feed the plasmonic phase modulator and extract the signal from it.

Exploring more complex simulation frameworks, the maximum realism could be achieved by 3D full-wave simulations of the entire device, which in principle can be carried out by commercially available electromagnetic simulators implementing general-purpose algorithms (*i.e.*,the finite-difference time-domain method - FDTD) such as RSoft FullWave[16] and Lumerical FDTD Solutions[17] (all of the 3D-FDTD simulations used in this work have been performed with the latter). Lumerical, starting from a defined field source (in this case the Si waveguide mode), returns the position-resolved 3D profile of the vectorial electromagnetic field on the entire device. As an example, Fig. 4 shows the top view of the real part of E_x in OFF (top), half-power (middle) and ON conditions,

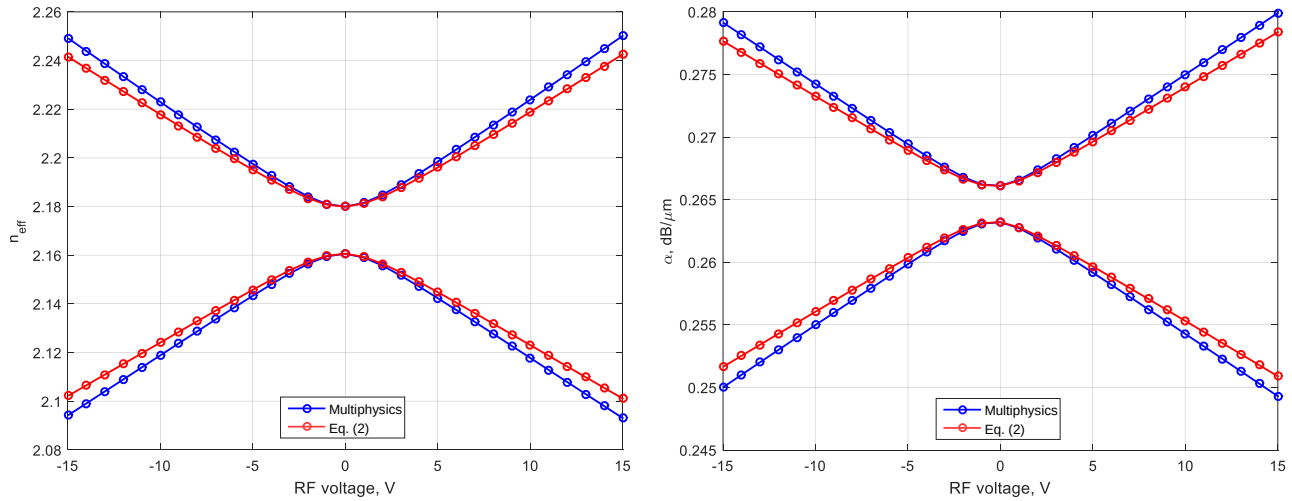

Figure 3. Effective refractive index n_{eff} (left) and attenuation coefficient α versus V_{RF}. Blue and red curves have been obtained from coupled quasi-static and optic simulations (multiphysics) and using the approximated expression (2), respectively.

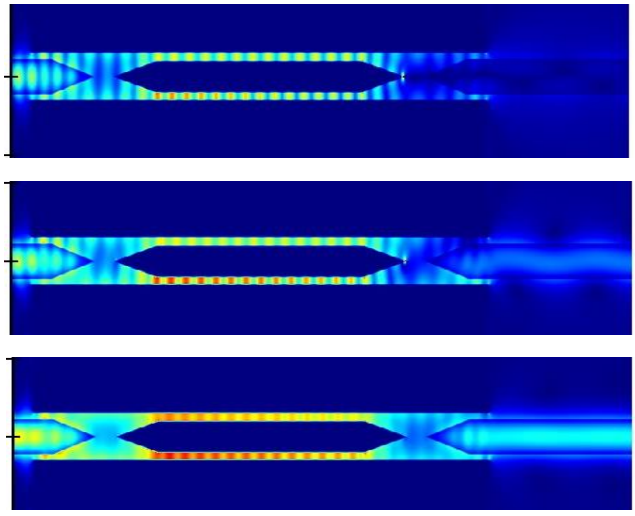

Figure 4. Color maps of the absolute value of the transverse electric field E_x from full 3D-FDTD simulations.[17] Above: OFF state; middle: half-power state; below: ON state.

which can be clearly recognized by inspecting the output beams. The MZM response can be defined by post-processing these field profiles. Because the modulator is embedded within a complex optical system featuring grating couplers and other components which can filter out spurious contributions, it is reasonable to base this definition on the fundamental mode of the output waveguide. By projecting the total (3D) field on it, a mode transmission coefficient S_{21} can be defined, whose absolute value squared can be interpreted as a $P_{\text{out}}/P_{\text{in}}$.

As in the previous section, each V_{RF} corresponds to a different FDTD simulation, which leads to staggering computation times (several days), for a single device. Hence, even considering that the compact footprint of POH MZMs makes such an *all-in-one* approach not impossible, it is still rather prohibitive. Aiming to minimize the number and the cost of the required 3D simulations, the following strategy has been conceived. Instead of modeling numerically the entire device, it is possible to focus the 3D-FDTD simulations only on the splitter/recombiner (which are actually equal, just mirrored). Then, the device response can be obtained by invoking the analogy of the MZM with the bimodal Fabry-Pérot interferometer (BFPI),[18,19] as shown in Fig. 5. The BFPI cavity features two transmission lines, representing the plasmonic modes supported by the

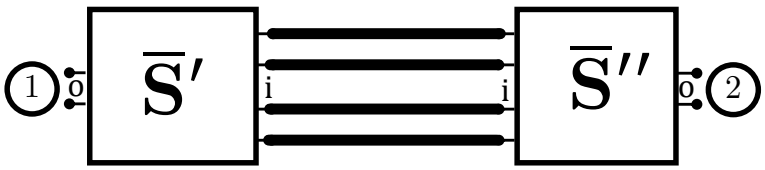

Figure 5. Distributed circuit representation of a bimodal Fabry-Pérot interferometer including the splitter (recombiner) scattering matrices $\overline{\mathbf{S}}'$ ($\overline{\mathbf{S}}''$) and the transmission lines modeling the phase modulator modes.

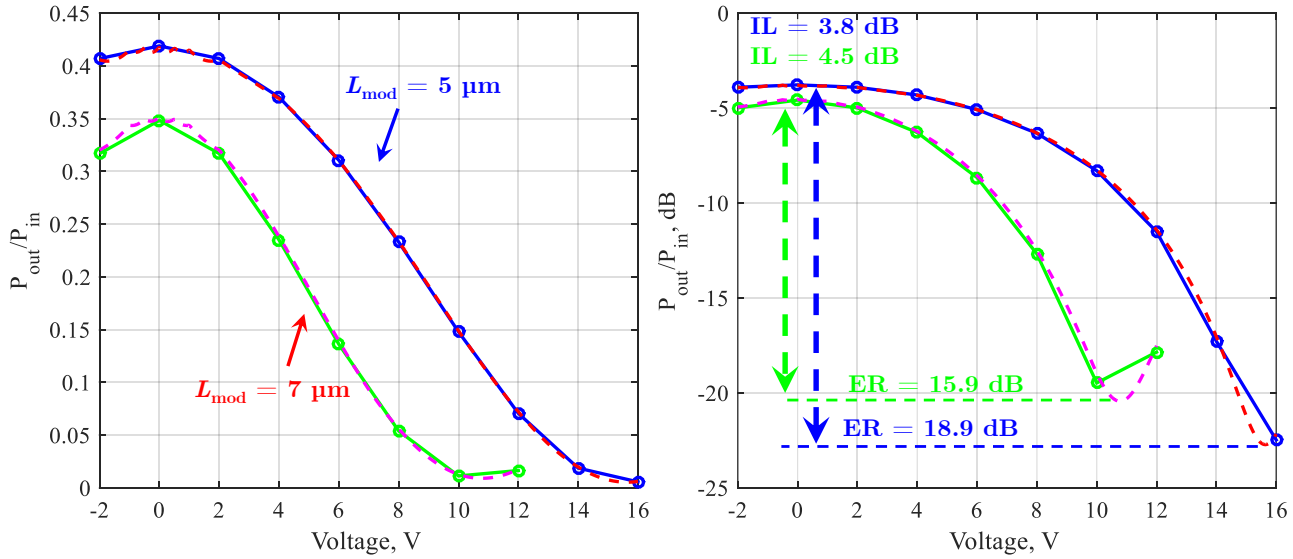

Figure 6. $P_{\mathrm{out}}/P_{\mathrm{in}}$ characteristics obtained with full 3D-FDTD simulations (solid lines and circular markers) and with the MFDTD approach presented in this work for two modulators with $L_{\mathrm{mod}} = 5\,\mu$m and $7\,\mu$m. The left and right panels show the results in linear and logarithmic scales, respectively.

MZM, coupled mutually and to the outer ports (fundamental Si waveguide modes) by 3×3 scattering matrices describing the splitter/recombiner.

The first step of this modal FDTD (MFDTD) *divide-et-impera* strategy requires simulating, with the 3D FDTD, only the section marked with the dashed cyan square in Fig. 1(left), at $V_{\mathrm{RF}} = 0\,\mathrm{V}$. This starts from the input waveguide, and is terminated at the end of the gold triangular taper. Then, the phase modulators can be modeled by the modal simulations discussed in Section 2, and cascaded to the splitter/recombiner to compute the full modulator response as the square magnitude of the transmission coefficient:

$$S_{21} = \overline{\mathbf{S}}''_{\mathrm{oi}} \left[\mathbf{I} - \overline{\mathbf{S}}'_{\mathrm{ii}} \overline{\mathbf{S}}''_{\mathrm{ii}}\right]^{-1} \overline{\mathbf{S}}'_{\mathrm{io}}$$

Additional details about this methodology can be found in.[13]

This approach has been applied to the simulation of two POH MZMs, as summarized in Fig. 6, which reports the $P_{\mathrm{out}}/P_{\mathrm{in}}$ characteristics in linear (left) and log (right) scales. The two devices differ only by the modulator lengths L_{mod}, which are 5 and $7\,\mu$m, corresponding to $V_\pi = 16\,\mathrm{V}$ and $11\,\mathrm{V}$, respectively. Despite the many modeling difficulties of this device ranging from the need for adequate optical models for metals, possible non-idealities in the structure manufacturing and not-perfectly known optical properties of the polymer refractive index, the results exhibit a good qualitative agreement with the literature[5] for both ILs and ERs. Moreover, the remarkable superposition of the full 3D-FDTD simulations (evaluated in a limited number of voltages and marked with solid lines and open bullets) with the MFDTD results (dashed lines) validate the approach, paving the way towards the effective, yet accurate modeling of these devices.

ACKNOWLEDGMENTS

Support from the project HIRPO2017030805 "Modelling of integrated Mach-Zehnder electro-optic modulators: from materials to system-level design" of HiSilicon is gratefully acknowledged.

REFERENCES

[1] Ayata, M., Fedoryshyn, Y., Heni, W., Baeuerle, B., Josten, A., Zahner, M., Koch, U., Salamin, Y., Hoessbacher, C., Haffner, C., Elder, D. L., Dalton, L. R., and Leuthold, J., "High-speed plasmonic modulator in a single metal layer," *Science* **358**, 630–632 (Nov. 2017).

[2] Haffner, C., Chelladurai, D., Fedoryshyn, Y., Josten, A., Baeuerle, B., Heni, W., Watanabe, T., Cui, T., Cheng, B., Saha, S., Elder, D. L., Dalton, L. R., Boltasseva, A., Shalaev, V. M., Kinsey, N., and Leuthold, J., "Low-loss plasmon-assisted electro-optic modulator," *Nature* **556**, 483–486 (2018).

[3] Haffner, C., Joerg, A., Doderer, M., Mayor, F., Chelladurai, D., Fedoryshyn, Y., Roman, C. I., Mazur, M., Burla, M., Lezec, H. J., Aksyuk, V. A., and Leuthold, J., "Nano–opto-electro-mechanical switches operated at CMOS-level voltages," *Science* **366**(6467), 860–864 (2019).

[4] Koos, C., Leuthold, J., Freude, W., Kohl, M., Dalton, L., Bogaerts, W., Giesecke, A. L., Lauermann, M., Melikyan, A., Koeber, S., Wolf, S., Weimann, C., Muehlbrandt, S., Koehnle, K., Pfeifle, J., Hartmann, W., Kutuvantavida, Y., Ummethala, S., Palmer, R., Korn, D., Alloatti, L., Schindler, P. C., Elder, D. L., Wahlbrink, T., and Bolten, J., "Silicon-organic hybrid (SOH) and plasmonic-organic hybrid (POH) integration," *J. Lightwave Technol.* **34**, 256–268 (Nov. 2015).

[5] Haffner, C., Heni, W., Fedoryshyn, Y., Josten, A., Baeuerle, B., Hoessbacher, C., Salamin, Y., Koch, U., Dordevic, N., Mousel, P., Bonjour, R., Emboras, A., Hillerkuss, D., Leuchtmann, P., Elder, D. L., Dalton, L. R., Hafner, C., and Leuthold, J., "Plasmonic organic hybrid modulators–scaling highest speed photonics to the microscale," *Proc. IEEE* **104**, 2362–2379 (Dec. 2016).

[6] Dalton, L. R., Sullivan, P. A., and Bale, D. H., "Electric field poled organic electro-optic materials: State of the art and future prospects," *Chem. Rev.* **110**, 25–55 (Oct. 2009).

[7] Elder, D. L., Benight, S. J., Song, J., Robinson, B. H., and Dalton, L. R., "Matrix-assisted poling of monolithic bridge-disubstituted organic NLO chromophores," *Chem. Mater.* **26**, 872–874 (Jan. 2014).

[8] Emboras, A., Hoessbacher, C., Haffner, C., Heni, W., Koch, U., Ma, P., Fedoryshyn, Y., Niegemann, J., Hafner, C., and Leuthold, J., "Electrically controlled plasmonic switches and modulators," *IEEE J. Select. Topics Quantum Electron.* **21**, 4600408 (July 2015).

[9] Haffner, C., Heni, W., Fedoryshyn, Y., Niegemann, J., Melikyan, A., Elder, D. L., Baeuerle, B., Salamin, Y., Josten, A., Koch, U., Hoessbacher, C., Ducry, F., Juchli, L., Emboras, A., Hillerkuss, D., Kohl, M., Dalton, L. R., Hafner, C., and Leuthold, J., "All-plasmonic Mach–Zehnder modulator enabling optical high-speed communication at the microscale," *Nature Photon.* **9**, 525–528 (July 2015).

[10] Heni, W., Haffner, C., Elder, D. L., Tillack, A. F., Fedoryshyn, Y., Cottier, R., Salamin, Y., Hoessbacher, C., Koch, U., Cheng, B., Robinson, B., Dalton, L. R., and Leuthold, J., "Nonlinearities of organic electro-optic materials in nanoscale slots and implications for the optimum modulator design," *Opt. Express* **25**, 2627–2653 (Feb. 2017).

[11] Bertazzi, F., Peverini, O. A., Goano, M., Ghione, G., Orta, R., and Tascone, R., "A fast reduced-order model for the full-wave FEM analysis of lossy inhomogeneous anisotropic waveguides," *IEEE Trans. Microwave Theory Tech.* **MTT-50**, 2108–2114 (Sept. 2002).

[12] Orta, R., Tibaldi, A., and Debernardi, P., "Bimodal resonance phenomena–part II: high/low-contrast grating resonators," *IEEE J. Quantum Electron.* **52**(12), 6600409–1–8 (2016).

[13] Tibaldi, A., Ghomashi, M., Bertazzi, F., Goano, M., Vallone, M., and Ghione, G., "Plasmonic-organic hybrid electro/optic Mach-Zehnder modulators: from waveguide to multiphysics modal-FDTD modeling," *Opt. Express* **28**, 29253–29271 (Sept. 2020).

[14] Bertazzi, F., Ghione, G., and Goano, M., "Efficient quasi-TEM frequency-dependent analysis of lossy multiconductor lines through a fast reduced-order FEM model," *IEEE Trans. Microwave Theory Tech.* **MTT-51**, 2029–2035 (Sept. 2003).

[15] Ghione, G., [*Semiconductor Devices for High-Speed Optoelectronics*], Cambridge University Press, Cambridge, U.K. (2009).

[16] Synopsys, Inc., Inc., Optical Solutions Group, Ossining, NY, *RSoft FullWAVE User Guide, v2017.03* (2017).
[17] Lumerical Inc. (2019).
[18] Orta, R., Tibaldi, A., and Debernardi, P., "Bimodal resonance phenomena–part I: generalized Fabry–Pérot interferometers," *IEEE J. Quantum Electron.* **52**(12), 6100508–1–8 (2016).
[19] Tibaldi, A., Debernardi, P., and Orta, R., "Bimodal resonance phenomena–part III: high-contrast grating reflectors," *IEEE J. Quantum Electron.* **54**(6), 6600108–1–8 (2018).